Crystal structure, phase transition and ferroelectric properties of the $[(CH_3)_3NH]_3[Sb_2Cl_{9(1-x)}Br_{9x}]$ (TMACBA) mixed crystals

2003 J. Phys.: Condens. Matter 15 5765

(http://iopscience.iop.org/0953-8984/15/33/310)

INSTITUTE OF PHYSICS PUBLISHING JOURNAL OF PHYSICS: CONDENSED MATTER

J. Phys.: Condens. Matter **15** (2003) 5765–5781 PII: S0953-8984(03)63775-6

Crystal structure, phase transition and ferroelectric properties of the $[(CH_3)_3NH]_3[Sb_2Cl_{9(1-x)}Br_{9x}]$ (TMACBA) mixed crystals

M Wojtaś[1], G Bator[1], R Jakubas[1,3] and J Zaleski[2]

[1] Faculty of Chemistry, University of Wrocław, Joliot-Curie 14, 50-383 Wrocław, Poland
[2] Institute of Chemistry, University of Opole, Oleska 48, 45-951 Opole, Poland

E-mail: rj@wchuwr.chem.uni.wroc.pl

Received 21 May 2003
Published 8 August 2003
Online at stacks.iop.org/JPhysCM/15/5765

Abstract

The paraelectric–ferroelectric phase transition in the $[(CH_3)_3NH]_3[Sb_2Cl_{9(1-x)}Br_{9x}]$ (TMACBA) mixed crystals is investigated by the differential scanning calorimetry, dilatometric and dielectric methods. The phase transition is found at 363.5, 362.7, 360.5 and 350.9 K (on cooling) for TMACBA crystals with $x = 0$, 0.02, 0.17 and 0.42, respectively. The crystal structures of the pure bromine analogue ($x = 1$), TMABA, and the mixed crystal TMACBA ($x = 0.55$) are determined at 297 K. TMABA crystallizes in the trigonal space group $R\bar{3}c$: $a = 15.098(2)$ Å, $c = 21.906(4)$ Å, $Z = 3$, $R_1 = 0.0393$, $wR_2 = 0.0746$. Its structure is built up of discrete $Sb_2Br_9^{3-}$ bioctahedra and disordered trimethylammonium cations. Ferroelectric TMACBA ($x = 0.55$) crystallizes in the monoclinic space group Pc: $a = 10.245(2)$ Å, $b = 9.122(2)$ Å, $c = 15.549(3)$ Å, $\beta = 90.52(3)°$, $Z = 2$, $R_1 = 0.0340$, $wR_2 = 0.0712$. The crystal is built of two-dimensional layer anions ('honeycomb-like structure') and three trimethylammonium cations. Dielectric studies on TMACBA ($x = 0.42$) in the frequency range 75 kHz–900 MHz indicate relatively fast reorientation of the trimethylammonium cations over the paraelectric phase. The ferroelectricity of mixed crystals is preserved for Br concentration smaller than 0.60 ± 0.05. The polar properties are strictly connected with the presence of the polyanionic layer structure. A possible mechanism for the paraelectric–ferroelectric phase transition in the TMACBA mixed crystals is discussed on the basis of the results presented.

1. Introduction

Ferroelectric crystals are interesting materials since they can be used e.g. as the non-linear elements in electrical circuits or non-volatile memories [1]. Their voltage and temperature

[3] Author to whom any correspondence should be addressed.

dielectric characteristics are thus of great importance. For many years we have been searching for new ferroelectric materials in the family of alkylammonium halogenoantimonates (III) and bismuthates (III) of the general formula $R_aM_bX_{(3b+a)}$ (R—alkylammonium cation, M—antimony (III) or bismuth (III), X—chlorine, bromine or iodine). In this family seven ferroelectric crystals have been discovered and extensively investigated [2–15].

From the crystallographic studies on the crystals from the family mentioned above, it is found that those with $R_3M_2X_9$ composition crystallize with four different anionic subunits. In each of these subunits the antimony (bismuth) atoms are in the centre of distorted octahedra. The octahedra may be connected with each other in such a way that they form either infinite one-dimensional chains, two-dimensional layers, discrete bioctahedral or four octahedral units [3]. The ferroelectric properties appear only in these crystals, which are built of two-dimensional layers ('honeycomb-like' structure) [2].

In particular, $[(CH_3)_3NH]_3[Sb_2Cl_9]$ (TMACA) is ferroelectric at room temperature. It undergoes two closely lying phase transitions to the paraelectric phase: at $T_{c1} = 364$ K and at $T_{c2} = 363$ K [16]. The very narrow phase between T_{c1} and T_{c2} was recognized as an incommensurate one. Below 363 K TMACA is a ferroelectric down to the liquid helium temperature [17, 18].

It is well known that the ferroelectric properties of the crystals may be modified by an exchange of the metal atoms (e.g. Sb $\rightarrow$ Bi) in the crystal lattice [19]. The substitution for the antimony atoms of the bismuth ones in TMACA remarkably affected the parameters of the paraelectric–ferroelectric phase transition. The increase of the Bi concentration in the mixed $[(CH_3)_3NH]_3[Sb_{2(1-x)}Bi_{2x}Cl_9]$ (TMACAB) crystals shifted the phase transition towards lower temperatures and simultaneously decreased the maximum value of ϵ_0 at T_C [20–23]. X-ray diffraction and dielectric studies on the mixed TMACAB crystals clearly showed that the existence of ferroelectric properties in the halogenoantimonates (III) of the $R_3M_2X_9$ composition was strictly related to the presence of polyanionic layer structure. Increase of the Bi atom concentration above $x = 0.33$ caused change of the anionic sublattice to discrete $M_2Cl_9^{3-}$ units and simultaneous disappearance of the high electric polarizability of the crystal.

For technical applications it is important that the ferroelectric properties appear in a convenient temperature range (i.e. close to room temperature). It is also desirable that the enhanced electric permittivity persists over a wide temperature region. It is also necessary to determine the frequency range in which the dielectric absorption appears. These are the reasons that we have undertaken studies on the effect of halogen atom substitution in ferroelectric TMACA crystals on the temperature and frequency characteristics of their electric permittivity.

These studies are believed also to contribute to a widening of knowledge about the nature of the paraelectric–ferroelectric phase transitions in the molecular–ionic crystals studied. In particular, the recognition of the effect of the layer anionic structure (its modification) on the dynamical dielectric properties and the value of the spontaneous polarization of these crystals is of great importance.

2. Experimental details

The single crystals of $[(CH_3)_3NH]_3[Sb_2Cl_9]$ (TMACA) were obtained by adding dry $(CH_3)_3N$ to an aqueous solution of $SbCl_3$ with an excess of HCl. The compound was recrystallized twice from the solution and the single crystals were grown at constant room temperature. Recrystallization of pure $[(CH_3)_3NH]_3[Sb_2Cl_9]$ from aqueous solutions containing HBr in various concentrations gave $[(CH_3)_3NH]_3[Sb_2Cl_{9(1-x)}Br_{9x}]$. The mixed crystals with $x < 0.55$

are isomorphous with pure TMACA crystal. Their morphologies are identical and the density of the mixed crystals changes linearly with the Br content. Mixed crystals with the following Br contents were obtained and studied: $x = 0$, 0.02, 0.17 and 0.42. Crystals with Bi content $x \geqslant 0.60 \pm 0.05$ were also obtained, for which no phase transitions were, however, detected. From this it may be concluded that the anionic layer structure disappeared and this Bi content may be approximately close to the limit of the existence of ferroelectricity in such crystals. The x-value was estimated on the basis of the density value. The same procedure was applied to grow the pure bromine analogue $[(CH_3)_3NH]_3[Sb_2Br_9]$ (TMABA).

Structure determinations of $[(CH_3)_3NH]_3[Sb_2Cl_{9(1-x)}Br_{9x}]$ ($x = 0.55$) and pure TMABA were performed on an Xcalibur CCD single-crystal diffractometer[4] with graphite monochromated Mo Kα radiation, $\lambda = 0.71073$ Å, at room temperature. The ω-scan technique was used with $\Delta\omega = 0.75°$ for one image. The structures were solved by the Patterson method and refined by a full-matrix least-squares method. The parameters of non-hydrogen atoms were refined using anisotropic temperature factors. The hydrogen atoms were included using standard geometric criteria and constrained to distances of 0.96 Å (C–H) and 0.90 Å (N–H). The positions of hydrogen atoms were refined using a riding model. Free variables were used to constrain the isotropic U-values of chemically equivalent hydrogen atoms to be equal. The SHELX-97 program [24] was used for structure solution and refinement. Crystal data and structure refinement for TMACBA ($x = 0.55$) and the pure bromine analogue, TMABA, are presented in table 1. The structure drawings were prepared using the SHELXTL program [25]. A list of calculated and observed structure factors may be obtained from the authors on request. Crystallographic data for the structures reported in this paper (excluding structure factors) have been deposited with the Cambridge Crystallographic Data Centre, CCDC Nos 208514 and 208515. Copies of this information may be obtained free of charge from the Director, CCDC, 12 Union Road, Cambridge CB2 1EZ, UK (fax: +44-1223-336033; e-mail: deposit@ccdc.cam.ac.uk or http://www.ccdc.cam.ac.uk).

Differential scanning calorimetry (DSC) was performed using a Perkin-Elmer DSC-7 in the temperature range 100–400 K with scanning rates from 5 to 20 K min^{-1}. The temperature of the phase transition was estimated by approximation to the scanning rate 0 K min^{-1}. The dilatometric measurements were made with a thermomechanical analyser, Perkin-Elmer TMA-7, over the temperature range 100–400 K with a rate 2 K min^{-1}. The dimensions of the sample were of the order of $4 \times 4 \times 1$ mm^3.

The complex electric permittivity, $\epsilon^* = \epsilon' - i\epsilon''$, between 295 and 370 K was measured using Agilent 4284A and HP 4285A Precision LCR Meters in the frequency range between 120 Hz and 30 MHz as well as a HP 4191A Impedance Analyser in the frequency range between 30 and 900 MHz. The dimensions of the samples were of the order of $4 \times 4 \times 1$ mm^3. The overall errors for the real and imaginary parts of the complex electric permittivity in the low- and high-frequency region were less than 5 and 10%, respectively.

The spontaneous polarization was measured between 295 and 370 K by a charge integration technique using a Keithley 617 Programmable Electrometer. The temperature was stabilized by temperature controller Instec STC200.

The Raman spectrum of the powder sample was recorded on a Nicolet Magna 860 FT Raman spectrometer. A diode-pumped Nd:YAG laser was the exciting source, with a power of about 200 mW. The backscattering geometry was used. The resolution was set as 2 cm^{-1}. 512 scans were measured.

[4] Oxford Diffraction, CrysAlis system software, CrysAlis CCD and CrysAlis RED, version 1.168 beta, Oxford Diffraction Ltd, 2001.

Table 1. Crystal data and structure refinement for TMACBA ($x = 0.55$) and the pure bromine analogue, TMABA.

Empirical formula	$[(CH_3)_3NH]_3[Sb_2Br_9]$	$[(CH_3)_3NH]_3[Sb_2Cl_{9(1-x)}Br_{9x}]$ ($x = 0.55$)
Formula weight (g mol^{-1})	1143.06	962.99
Temperature (K)	297(2)	297(2)
Wavelength (Å)	0.710 73	0.710 73
Crystal system, space group	Trigonal, $R\bar{3}c$	Monoclinic, Pc
Unit cell dimensions		
a (Å)	15.098(2)	10.245(2)
b (Å)	15.098(2)	9.122(2)
c (Å)	21.906(4)	15.549(3)
β (deg)		90.52(3)
Volume (Å^3)	4324.5(11)	1453.1(5)
Z, calculated density (g cm^{-3})	3, 2.634	2, 2.201
Absorption coefficient (mm^{-1})	14.349	9.038
$F(000)$	3132	898
Crystal size (mm^3)	$0.20 \times 0.20 \times 0.20$	$0.40 \times 0.40 \times 0.20$
θ-range for data collection (deg)	3.63–29.68	3.26–29.75
Index ranges	$-20 \leqslant h \leqslant 16$, $-20 \leqslant k \leqslant 20$, $-29 \leqslant l \leqslant 30$	$-14 \leqslant h \leqslant 14$, $-8 \leqslant k \leqslant 12$, $-21 \leqslant l \leqslant 21$
Reflections collected/unique	11 189/2529 (R(int) = 0.0594)	11 514/7052 (R(int) = 0.0208)
Completeness to 2θ (%)	29.68, 97.2	29.75, 91.7
Max. and min. transmission	0.1615 and 0.1615	0.2651 and 0.1227
Refinement method	Full-matrix least-squares fit on F^2	
Data/restraints/parameters	2529/1/80	7052/2/273
Goodness-of-fit on F^2	0.907	0.891
Final R-indices ($I > 2\sigma(I)$)	$R_1 = 0.0393$, $wR_2 = 0.0746$	$R_1 = 0.0340$, $wR_2 = 0.0712$
R-indices (all data)	$R_1 = 0.0630$, $wR_2 = 0.0831$	$R_1 = 0.0493$, $wR_2 = 0.0759$
Absolute structure parameter	0.045(16)	0.51(1)
Largest diff. peak and hole (e Å^{-3})	0.750 and −1.140	0.753 and −0.869

3. Results

3.1. X-rays

The atomic coordinates and equivalent isotropic displacement parameters for TMABA are presented in table 2. The crystal structure of TMABA is composed of one crystallographically independent discrete bioctahedral $Sb_2Br_9^{3-}$ unit consisting of two $SbBr_6^{3-}$ octahedra connected by faces. Three bromine atoms of each octahedron are bridging and three are terminal. Each bridging bromine atom is located opposite to the terminal one. Bioctahedral anionic moieties in TMABA crystal are presented in figure 1(a).

The Sb–Br bond lengths are listed in table 3. Generally, the bridging bonds are much longer than the terminal ones, which is the case also for the other halogenoantimonates (III). The terminal bonds are between 2.547(1) and 2.618(1) Å, whereas the bridging ones are between 3.003(1) and 3.191(1) Å. Taking into account the difference in bond lengths, we may conclude that the first octahedron (around Sb(1)) is much less deformed that the other one (around Sb(2)). The difference between the terminal and bridging bonds for the first octahedron is 0.391(1) Å. The other octahedron shows larger deformation, with differences between bridging and terminal bonds equal to 0.644 Å. The Br–Sb–Br angles for mutual *cis*-bonds vary from 80.00(3)° to 99.15(3)°. There is one independent trimethylammonium cation

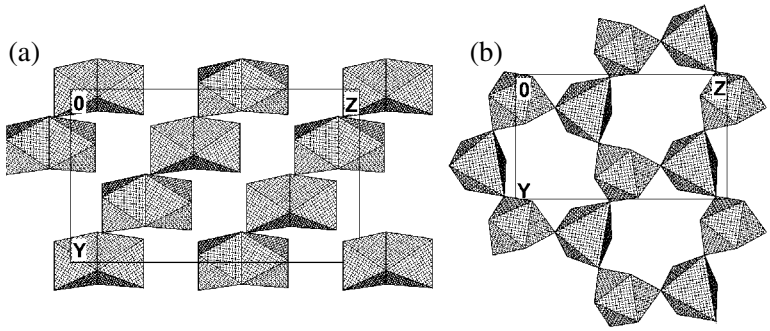

Figure 1. (a) The bioctahedral anionic sublattice in TMABA and (b) a two-dimensional layer anionic structure for the mixed TMACBA crystals.

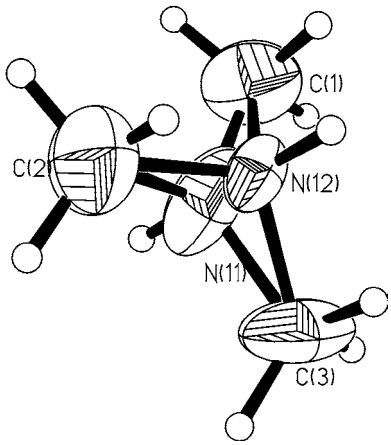

Figure 2. Cationic disorder with the atom numbering in the crystal structure of TMABA.

in the crystal structure. It is disordered, possessing two positions for the nitrogen atom with occupancy factors 0.30 for N(11) and 0.70 for N(12). The picture of the cation is presented in figure 2. This type of disorder may be a result of the overall reorientation of the cation along the axis passing through one of the carbon atoms and the centre of gravity of the molecule. The trimethylammonium cations are connected to the anions by very weak hydrogen bonds, with N–H $\cdots$ Br distances longer than 3.5 Å.

The atomic coordinates and equivalent isotropic displacement parameters for $[(CH_3)_3NH]_3[Sb_2Cl_{9(1-x)}Br_{9x}]$ ($x = 0.55$) (TMACBA) are presented in table 2. The anionic sublattice of this system is built of characteristic two-dimensional 'honeycomb' layers lying in the *bc*-plane (figure 1(b)). These layers are composed of distorted SbX_6^{3-} (X = Cl or Br) octahedra connected with each other by corners forming 12-membered $(X–Sb–X)_6$ rings. In the coordination sphere of each octahedron there are three bridging and three terminal Sb–X bonds. The SbX_6^{3-} octahedra are significantly distorted. The Sb–Cl terminal bond lengths are between 2.429(3) and 2.544(3) Å, whereas the Sb–Br terminal bonds are between 2.450(6) and 2.651(3) Å. The bridging Sb–Br bonds are between 3.012(1) and 3.279(1) Å. Similarly to in the other alkylammonium halogenoantimonates (III), the elongation of any particular Sb–X bond leads to a shortening of the bond located opposite. As expected, the longest terminal Sb–Br bond, Sb(1)–Br(3) (2.590(2) Å), in the Sb(1) octahedron lies opposite to the shortest

Table 2. Atomic coordinates (units of 10^4) and equivalent isotropic displacement parameters (units of 10^3 Å^2) for $[(CH_3)_3NH]_3[Sb_2Br_9]$ (TMABA) and $[(CH_3)_3NH]_3[Sb_2Cl_{9(1-x)}Br_{9x}]$ ($x = 0.55$) (TMACBA). U(eq) is defined as one third of the trace of the orthogonalized U_{ij}-tensor. O is the final percentage of occupancy of sites shared by either nitrogen atoms (TMABA and TMACBA) or by chlorine and bromine atoms (TMACBA).

	x	y	z	U(eq)	O
			TMABA		
Sb(1)	10 000	10 000	5080(1)	28(1)	
Sb(2)	10 000	10 000	6899(1)	037(1)	
Br(1)	8 383(1)	8 804(1)	4427(1)	52(1)	
Br(2)	9 519(1)	8 247(1)	5923(1)	42(1)	
Br(3)	8 522(1)	8 648(1)	7527(1)	67(1)	
N(11)	6 390(9)	6 710(4)	6097(18)	70(2)	0.30
N(12)	6 983(18)	6 986(14)	5972(8)	36(4)	0.70
C(1)	6 627(9)	6 272(8)	6529(5)	66(3)	
C(2)	6 524(9)	6 363(9)	5422(6)	80(4)	
C(3)	6 705(10)	7 760(8)	6054(6)	72(3)	
			TMACBA		
Sb(1)	84(1)	2 098(1)	29(1)	38(1)	
Sb(2)	−3 134(1)	7 145(1)	−1696(1)	40(1)	
Cl(1)	1 267(4)	49(5)	759(3)	107(2)	0.73
Cl(2)	1 301(2)	1 628(2)	−1297(2)	32(1)	0.56
Cl(3)	1 654(3)	4 059(3)	570(2)	47(1)	0.56
Cl(7)	−4 328(3)	5 358(3)	−2576(2)	53(1)	0.73
Cl(8)	−4 512(4)	9 093(4)	−2310(3)	88(1)	0.73
Cl(9)	−4 706(3)	6 748(3)	−560(2)	53(1)	0.73
Br(1)	1 287(3)	146(3)	784(2)	41(1)	0.27
Br(2)	1 400(4)	1 686(5)	−1278(2)	149(2)	0.44
Br(3)	1 896(2)	3 953(2)	449(1)	52(1)	0.44
Br(7)	−4 389(6)	5 413(6)	−2580(4)	113(2)	0.27
Br(8)	−4 362(3)	9 236(4)	−2370(3)	58(1)	0.27
Br(9)	−4 890(3)	6 855(4)	−466(2)	45(1)	0.27
Br(4)	−1 829(1)	−224(1)	−538(1)	65(1)	1.00
Br(5)	−1 193(1)	7 333(1)	−3142(1)	73(1)	1.00
Br(6)	−1 503(1)	4 487(1)	−1075(1)	77(1)	1.00
N(1)	−4 529(6)	1 805(6)	−273(4)	70(2)	
C(1)	−5 425(8)	671(8)	75(6)	106(3)	
C(2)	−4 161(10)	2 799(10)	404(5)	118(3)	
C(3)	−5 044(9)	2 524(8)	−1011(5)	90(3)	
N(21)	−1 596(10)	3 104(10)	−3179(5)	48(3)	0.58
N(22)	−1 386(16)	2 258(17)	−3620(10)	107(5)	0.42
C(4)	−1 464(12)	1 523(10)	−2860(7)	172(4)	
C(5)	−215(9)	3 205(11)	−3391(7)	140(4)	
C(6)	−2 067(14)	3 338(15)	−3911(8)	221(6)	
N(3)	1 470(5)	6 933(5)	−1849(4)	64(2)	
C(7)	1 990(7)	5 500(7)	−1917(6)	86(3)	
C(8)	1 237(9)	7 376(8)	−968(6)	99(3)	
C(9)	2 293(9)	7 994(8)	−2288(6)	97(3)	

bridging one, Sb(1)–Br(4) (3.012(1) Å), in this octahedron. Similarly, the longest bridging bond in this octahedron, Sb(1)–Br(6) (3.208(1) Å), lies opposite to the shortest terminal one, Sb(1)–Br(1) (2.458(3) Å). The same situation arises in the other octahedron. The terminal

Table 3. Selected bond lengths (Å) and angles (deg) for $[(CH_3)_3NH]_3[Sb_2Br_9]$ (TMABA) and $[(CH_3)_3NH]_3[Sb_2Cl_{9(1-x)}Br_{9x}]$ ($x = 0.55$) (TMACBA).

TMABA			
Sb(1)–Br(1)	2.618(1)	Br(1) No 2–Sb(1)–Br(2) No 1	175.09(4)
Sb(1)–Br(2)	3.003(1)	Br(2) No 2–Sb(1)–Br(2) No 1	86.15(3)
Sb(2)–Br(2)	3.191(1)	Br(3) No 2–Sb(2)–Br(3) No 1	93.52(4)
Sb(2)–Br(3)	2.547(1)	Br(3) No 2–Sb(2)–Br(2)	99.15(3)
Br(2) No 2–Sb(1)–Br(2)	86.15(3)	Br(3) No 1–Sb(2)–Br(2)	167.23(4)
Br(1)–Sb(1)–Br(2) No 1	90.80(3)	Br(3)–Sb(2)–Br(2)	87.29(3)
Symmetry transformations used to generate equivalent atoms: No 1: $-x+y+1, -x+2, z$; No 2: $-y+2, x-y+1, z$			
TMACBA			
Sb(1)–Br(1)	2.458(3)	Sb(2)–Br(6)	3.094(1)
Sb(1)–Br(2)	2.478(4)	Sb(2)–Br(5)	3.020(1)
Sb(1)–Br(3)	2.590(2)	Br(2)–Sb(1)–Br(6)	86.62(9)
Sb(1)–Cl(1)	2.495(4)	Br(3)–Sb(1)–Br(4)	174.70(5)
Sb(1)–Cl(2)	2.457(3)	Br(3)–Sb(1)–Br(6)	92.84(5)
Sb(1)–Cl(3)	2.544(3)	Br(4)–Sb(1)–Br(5) No 1	96.00(3)
Sb(1)–Br(4)	3.012(1)	Br(4)–Sb(1)–Br(6)	89.75(3)
Sb(1)–Br(6)	3.208(1)	Br(5) No 1–Sb(1)–Br(6)	99.00(3)
Sb(2)–Cl(7)	2.449(3)	Cl(8)–Sb(2)–Br(4) No 2	85.06(10)
Sb(2)–Cl(8)	2.457(4)	Cl(9)–Sb(2)–Br(4) No 2	88.83(7)
Sb(2)–Cl(9)	2.429(3)	Cl(7)–Sb(2)–Br(5)	87.18(7)
Sb(2)–Br(7)	2.450(6)	Cl(9)–Sb(2)–Br(5)	174.60(7)
Sb(2)–Br(8)	2.509(4)	Cl(7)–Sb(2)–Br(6)	85.33(7)
Sb(2)–Br(9)	2.651(3)	Cl(8)–Sb(2)–Br(6)	174.12(10)
Symmetry transformations used to generate equivalent atoms: No 1: $x, -y+1, z+1/2$; No 2: $x, y+1, z$; No 3: $x, y-1, z$; No 4: $x, -y+1, z-1/2$			

chlorines/bromines are free to adjust to minimize the interaction energy. Two out of three non-equivalent $[(CH_3)_3NH]^+$ trimethylammonium cations (TMA(1), TMA(3)) are located between the inorganic layers. The third one (TMA(2)) occupies the cavity inside the $(X–Sb–X)_6$ ring and is distributed between two sites with occupancy factors 0.58 and 0.42.

It should be emphasized that this distribution is related to the presence of the domain structure of the crystal studied, not to dynamical disorder of this cation. It should be added that the determination of the structure was performed assuming that the bridging positions are occupied only by bromine atoms. When an attempt was made to add the chlorine atoms at the bridging positions, the occupancy factors for those chlorine atoms went to zero. The assumption mentioned above affects the estimation of the Br concentration in the mixed crystal (the accuracy is of the order of several per cent) and in consequence the calculated density may differ from the real one. It should be emphasized that this is a rare example of a crystal structure determination for mixed crystals containing both heavy metals (Sb(III)) and partially substituted halogen atoms.

3.2. Thermal behaviour of TMACBA

In order to detect the structural phase transition in $[(CH_3)_3NH]_3[Sb_2Cl_{9(1-x)}Br_{9x}]$ (TMACBA) ($x = 0.02$, 0.17 and 0.42), DSC and dilatometric measurements have been undertaken. The DSC curves obtained for TMACBA ($x = 0.02$, 0.17 and 0.42) crystals during cooling and

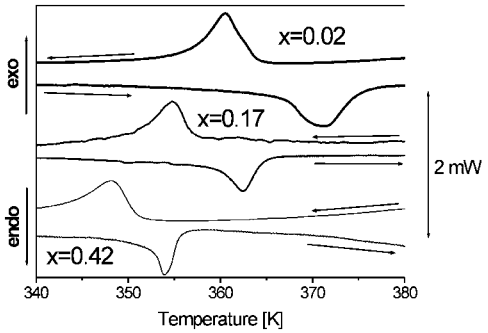

Figure 3. DSC curves for the TMACAB crystals with various Br contents: $x = 0.02$, 0.17 and 0.42 for cooling and heating runs (10 K min^{-1}).

Table 4. DSC data for the mixed TMACBA crystals with various Br contents (x). T_c and ΔS stand for the transition temperature (taken during cooling) and the transition entropy, respectively.

x	T_c (K)	ΔT (K)	ΔS (J mol^{-1} K^{-1})
0	363.5	5.1	4.57
0.02	362.7	3.2	4.33
0.17	358.2	2.2	3.34
0.42	350.9	1.7	3.30

heating scans are presented in figure 3. The DSC results show that we are dealing with one reversible phase transition of first-order type at 363.5, 362.7, 358.2 and 350.9 K (on cooling) for TMACBA crystals with $x = 0, 0.02, 0.17$ and 0.42, respectively. The temperatures of the phase transitions as well as the transition entropy values are collected in table 4. The entropy values, ΔS, indicate the 'order–disorder' type of the phase transitions observed. The temperature hysteresis (ΔT) extrapolated to zero scanning rate depends on the Br atom concentration; with increase of the x-value, the value of ΔT becomes smaller. This means that the character of the phase transition changes from a clear first-order type to a weak first-order one.

Figure 4 shows the results on the thermal expansion, $\Delta L/L_0$, for pure TMACA and TMACBA ($x = 0.42$) measured along the main crystallographic axes a, b and c on cooling (the directions presented correspond to those taken for the monoclinic room temperature phase). Stepwise changes in dimensions of the TMACA crystal are clearly seen at 363.5 K along the b- and c-axes. The changes in the $\Delta L/L_0$ values at T_C are of the order of 5×10^{-3}. The anomaly observed along the a-axis, which is normal to the cleavage plane b–c, is most probably related to partial cracking of the single crystals. It was observed for all samples for which measurements were taken along this axis. It is interesting that the average temperature coefficient of the linear thermal expansion, $\bar{\alpha} = \Delta L/L_0\,\Delta T$, for the b-axis is negative, whereas for the a- and c-directions it is positive. The lower part of figure 4 shows the temperature dependence of $\Delta L/L_0$ for the TMACBA crystals with $x = 0.42$. In addition to the fact that the temperature of the dilation anomalies is shifted towards lower temperature (350.9 K), the observed stepwise changes in $\Delta L/L_0$ are approximately five times lower than those for the pure TMACA crystal. It is interesting that along the a-axis the anomaly in the dilation is quite clearly visible. The linear thermal expansion coefficient, α, for all directions of the crystal investigated, is positive both above and below T_C. The values of $\bar{\alpha}$ along the main crystallographic directions are collected in table 5. The pressure coefficients for the first-order phase transitions estimated from the Clausius–Clapeyron relation: $\frac{dT_c}{dp} = \frac{\Delta V}{\Delta S}$ (where ΔS is

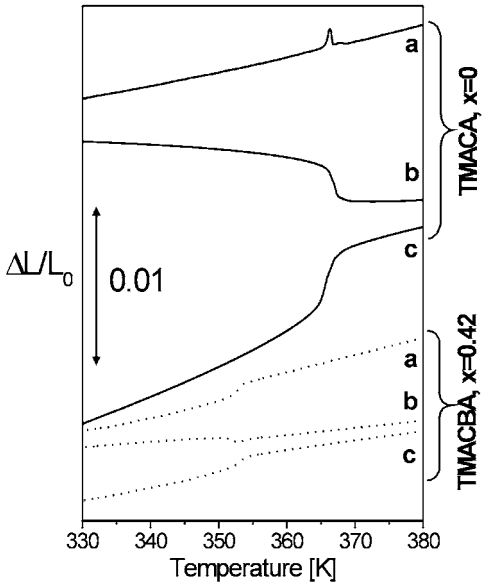

Figure 4. Temperature dependences of the thermal expansions for samples with $x = 0$ and 0.42 on cooling.

Table 5. Values of $\alpha = \Delta L/L_0\,\Delta T$ for pure TMACA crystals in the ferroelectric ('Ferro') and paraelectric ('Para') phases.

Direction:		*a*		*b*		*c*	
x	Phase	Ferro	Para	Ferro	Para	Ferro	Para
0	α (K^{-1})	8.94×10^{-5}	1.14×10^{-4}	-1.51×10^{-5}	3.26×10^{-5}	1.85×10^{-4}	1.01×10^{-4}
0.42	α (K^{-1})	6.46×10^{-5}	1.12×10^{-4}	3.47×10^{-5}	4.66×10^{-5}	7.05×10^{-5}	5.97×10^{-5}

the value of the transition entropy) are positive and amount to +0.33 and +0.30 K MPa^{-1} for the TMACA and TMACBA crystals, respectively.

3.3. Static and dynamic dielectric properties of TMACBA ($x = 0.42$) and TMABA

It is important to investigate the effect of the halogen atom substitution on the dielectric properties of mixed TMACAB crystals. Figure 5 shows the temperature dependences of the static electric permittivity, ϵ_c, for several mixed TMACBA crystals as well as for pure TMACA and TMABA. On the basis of the dielectric results presented, it may be stated that the substitution for Cl atoms of Br ones in TMACA remarkably affects the parameters of the paraelectric–ferroelectric phase transition. The increase of the Br concentration in TMACBA shifts the phase transition towards lower temperatures and simultaneously decreases the maximum value of ϵ_0 at T_C. We performed measurements of the complex electric permittivity, ϵ^*, for the $[(CH_3)_3NH]_3[Sb_2Cl_{9(1-x)}Br_{9x}]$ ($x = 0.42$) mixed crystals as a function of temperature and frequency as well. The purpose of these measurements was to determine the effect of the bromine content on the dielectric relaxation time, τ, and the corresponding energy of activation, E_a, for the dielectric relaxation processes. In the case of TMACA and isostructural mixed crystals, the dielectric measurements were performed along

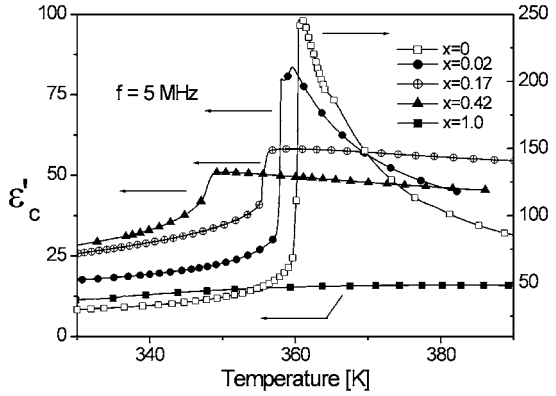

Figure 5. Temperature dependences of ϵ' for TMACBA crystals with the Br contents $x = 0$, 0.02, 0.17, 0.39, 0.42, 1.0 measured along the c-axis.

the monoclinic c-axis. Figure 6 shows the temperature dependences of ϵ'_c and ϵ''_c for mixed TMACBA ($x = 0.42$) on heating. Figure 7 presents the respective Cole–Cole diagrams over the paraelectric phase. It was found that the dielectric relaxation in TMACBA crystals is well described by the Cole–Cole relation:

$$\epsilon^* = \epsilon_\infty + \frac{\epsilon_0 - \epsilon_\infty}{1 + (\mathrm{i}\omega\tau)^{1-\alpha}}, \tag{1}$$

where ϵ_0 and ϵ_∞ are the low- and high-frequency limits of the electric permittivity, respectively, ω is the angular frequency, τ is the macroscopic relaxation time, α is the distribution of relaxation times parameter. The values of ϵ_0, ϵ_∞, τ and α were fitted for each temperature independently. The activation energy, E_a, was calculated according to the Arrhenius equation:

$$\tau_0 = C \exp\left(\frac{E_\mathrm{a}}{kT}\right), \tag{2}$$

where C is a constant. It is well known that in the case of the order–disorder ferroelectrics exhibiting critical slowing down, the activation energy is estimated from the temperature dependence of the microscopic relaxation time, τ_0. The relationship between the macroscopic, τ, and microscopic, τ_0, relaxation times is the following:

$$\tau_0 = \frac{\epsilon_\infty}{\epsilon_0 - \epsilon_\infty}\tau. \tag{3}$$

In our case the temperature dependence of the dielectric increment, $\Delta\epsilon$, is very weak, so we decided to use (2).

It should be mentioned that the value of the activation energy calculated in the way described above is burdened by relatively large error, which may be of the order of 20%. The replacement of the Cl atoms by the Br ones apparently also affects the dynamical dielectric properties of ferroelectric mixed crystals, which are isomorphous with the pure antimony analogue. The value of the relaxation time, τ, in the vicinity of the paraelectric–ferroelectric phase transition is almost one order lower than that in pure TMACA [19]. The value of the activation energy, $E_\mathrm{a} = 20$ kJ mol^{-1}, estimated from the Arrhenius relation for the macroscopic relaxation time is typical for the crystals, where we are dealing with reorientation of small alkylammonium cations [19, 20, 26, 27]. No significant distribution of the macroscopic relaxation times is observed, even in the vicinity of T_C, for mixed crystals ($\alpha < 0.1$) in

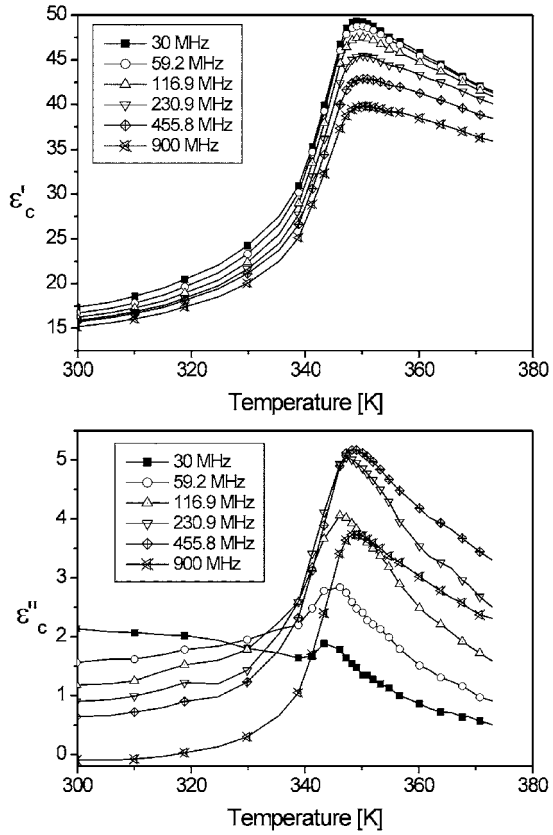

Figure 6. Temperature dependences of ϵ_c^* and ϵ_c^* for TMACBA crystals with the Br content $x = 0.42$ in the frequency range between 30 and 900 MHz.

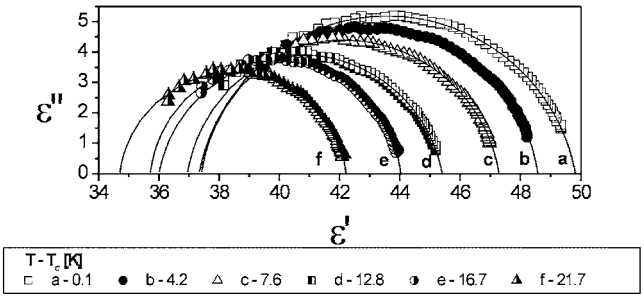

Figure 7. Cole–Cole diagrams for TMACBA crystals with the Br content $x = 0.42$ in the paraelectric phase.

comparison to the pure TMACA analogue, in which the distribution of relaxation times is more pronounced.

The relatively high value of $\epsilon_{\infty 1}$ as well as its strong temperature dependence for the mixed TMACBA ($x = 0.42$) crystals in the paraelectric phase indicate an additional higher-frequency relaxation mode. A similar situation was observed for the other trimethylammonium mixed crystals, in which antimony atoms were replaced by bismuth ones [19].

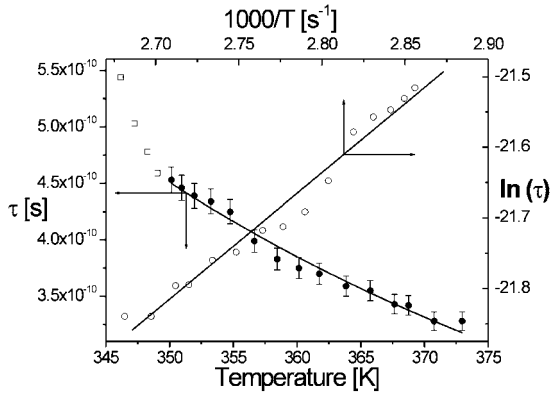

Figure 8. The temperature dependence of the macroscopic relaxation time τ (left and bottom) and $\ln(\tau)$ versus T^{-1} (right and top) in the vicinity of the paraelectric–ferroelectric phase transition ($T_C = 350.9$ K) for the TMACBA crystals with the Br content $x = 0.42$.

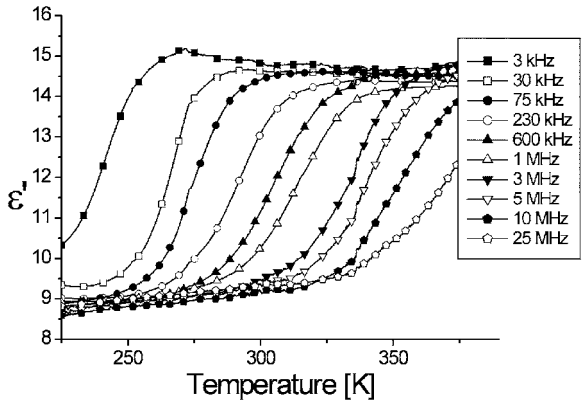

Figure 9. Temperature dependences of ϵ' for the TMABA crystal in the frequency range 3–25 MHz.

When the Br content exceeds about 60% the ferroelectric properties of the TMACBA mixed crystals disappear. Moreover, in the pure bromine analogue, TMABA, no structural phase transition is detected either by DSC or dilatometric methods. The complex electric permittivity measured between 3 kHz and 25 MHz along the *c*-axis for TMABA is displayed in figure 9. Such a dielectric response is typical for a simple dielectric relaxation process. The estimated activation energy for this process is equal to 55 kJ mol^{-1} and is comparable with that for the non-ferroelectric relaxation mode found in TMACA in the low-temperature region [28]. The analysis of the dielectric relaxation process in non-ferroelectric mixed TMACBA crystals will be published elsewhere [29].

3.4. Spontaneous polarization measurements

Measurements of the spontaneous polarization, P_s, were undertaken to analyse the influence of the bromine content on the value of P_s in the ferroelectric phase of TMACBA crystals with $x < 0.6$. The temperature dependences of P_s for the pure TMACA crystal and for TMACBA ($x = 0.42$) are displayed in figure 10. P_s versus temperature for pure TMACA is

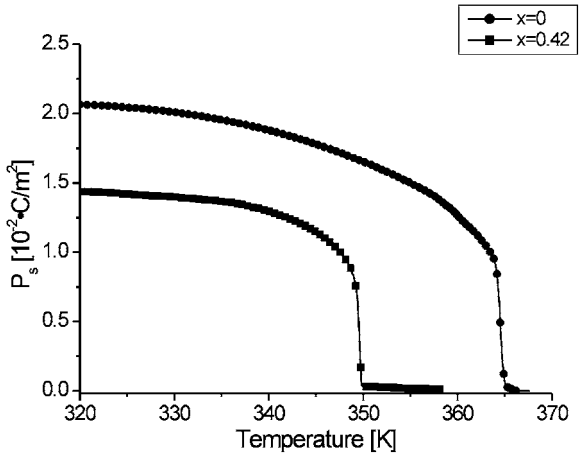

Figure 10. Temperature dependences of the spontaneous polarization P_s for pure TMACA and mixed TMACBA, $x = 0.42$, crystals.

typical of a first-order phase transition—at T_C an almost stepwise change in the polarization is observed. The replacement of chlorine atoms by bromine ones in the lattice of TMACA causes a reduction of the P_s-value (from about 2×10^{-2} C m^{-2} for pure TMACA to 1.5×10^{-2} C m^{-2} for TMACBA with $x = 0.42$). It should be noted that no 'tail' of the polarization value at the phase transition point is observed for the mixed crystals. It was found also that poling of the mixed TMACBA crystals up to ± 100 V does not change the value of P_s. This indicates that the crystals are most probably in a mono-domain state or the coercive field is relatively large.

3.5. Raman spectra

It is interesting to compare the Raman spectra of pure TMACA, TMABA and the mixed TMACBA crystals in the wavenumber region corresponding to the $Sb_2X_9^{3-}$ anionic modes. The Raman spectra in the low-frequency region for TMACA, TMACBA ($x = 0.42$) and TMABA crystals are shown in figure 11. In this wavenumber region the stretchings $\nu(Sb_2Cl_9^{3-})$ (at 325 and 264 cm^{-1}, TMACA) and $\nu(Sb_2Br_9^{3-})$ (at 207 and 181 cm^{-1}, TMABA) modes are observed. In the Raman spectra of TMACA and TMABA, double $\nu(Sb_2Cl_9^{3-})$ and $\nu(Sb_2Br_9^{3-})$ bands are observed due to the existence of terminal and bridging Sb–X bonds [30–32]. In the spectra of TMACA the bands at 160 and 147 cm^{-1} correspond to the deformation $\delta(Sb_2Cl_9^{3-})$ vibrations.

In the Raman spectra of the mixed TMACBA crystals, bands are observed which correspond both to $Sb_2Cl_9^{3-}$ and $Sb_2Br_9^{3-}$ stretching vibrations (314, 277, 204, 189 cm^{-1}). If we assume that in the wavenumber region 350–170 cm^{-1} we are really observing bands assignable to the vibrations of both the terminal and bridging Sb–X bonds, it is clearly seen that in the mixed crystals we are dealing with Cl atoms occupying both positions, terminal and bridging.

4. Discussion

Studies on the substitution effect for the $[(CH_3)_3NH]_3[Sb_2Cl_9]$ crystals were carried out in two directions. We have replaced Sb atoms by Bi ones or Cl atoms by Br ones. The problem

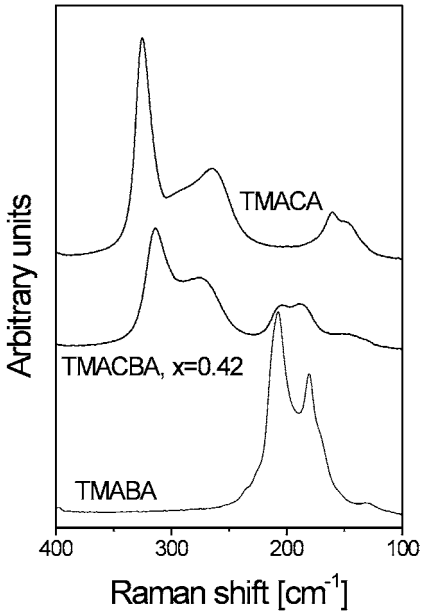

Figure 11. Raman spectra of pure TMACA, mixed TMACBA ($x = 0.42$) and pure TMABA crystals in the lattice vibrations range.

is to establish to what extent the deformation of the anionic sublattice affects the ferroelectric properties of the TMACA mixed analogues.

The situation in TMACBA is illustrated schematically in a diagram (see figure 12). It was clearly shown that substitution for Sb atoms with Bi ones or Cl atoms with Br ones leads to continuous deformation of the layer anionic structure. In both cases the $(M_2X_9^{3-})_\infty$ layer structure is destroyed when the x-parameter approaches either 0.33 for the Bi content or about 0.55 for the Br content and simultaneously ferroelectricity disappears. It is very interesting that the structures of pure $[(CH_3)_3NH]_3[Bi_2Cl_9]$ and $[(CH_3)_3NH]_3[Sb_2Br_9]$ crystals and their mixed analogues ($x_{Bi} > 0.33$ and $x_{Br} > 0.55$) are characterized by discrete $M_2X_9^{3-}$ moieties and all these salts crystallize in the same trigonal space group $R\bar{3}c$. Additionally, all these analogues possess quite similar static and dynamic dielectric properties. None of the mixed and pure analogues crystallizing in trigonal symmetry undergo any structural phase transitions. In the structure of these systems, one type of disordered trimethylammonium cation appears (placed in the general positions in the crystal lattice) and, on cooling, restriction of their motion proceeds continuously and does not lead to breaking of the crystal symmetry. The dynamic parameters of the dielectric relaxator identified with this cation in all non-ferroelectric crystals, such as the macroscopic relaxation time and the activation energy, are comparable in spite of the significant difference in dimensions of the $Bi_2Cl_9^{3-}$ and $Sb_2Br_9^{3-}$ moieties.

When taking into account the two ways in which the anionic layers deform, i.e. through metal (Sb $\rightarrow$ Bi) or halogen (Cl $\rightarrow$ Br) atom substitution, it should be noted that metal substitution affects the ferroelectric properties of the mixed crystals significantly more strongly. The change in the transition temperature and the reduction of the spontaneous polarization value are more remarkable and, what is more important, the destruction of the layer structure follows at lower x-values when the Sb is replaced by Bi in comparison to the Cl $\rightarrow$ Br exchange. This unequivocally shows that the metal atoms play a more important role in the polarizability

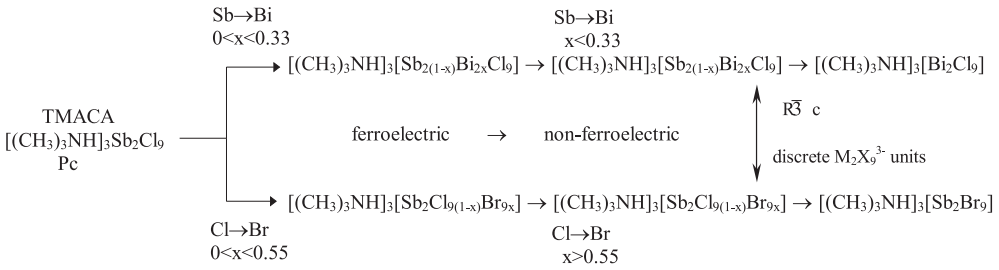

Figure 12. The phase diagram of the mixed TMACAB and TMACBA crystals.

of the layer structure than the halogen ones. Most probably this is related to the presence of the $5s^2$ electron pair of the Sb(III) atom. The results of x-ray and calorimetric studies, as well as the results of dielectric dispersion studies obtained up to now for pure TMACA crystals and the mixed analogue TMACAB ($x = 0.42$), allow us to propose a mechanism for the paraelectric–ferroelectric phase transition. The temperature evolution of the motional state for the trimethylammonium cations (TMA) in the paraelectric (MHT) and ferroelectric (MLT) phases is illustrated schematically in table 6. The evolution of the occupation factors for the two-site model is used to describe the disordering of the TMA cations. According to the crystallographic symmetry, two equivalent cations in the MHT phase generate two inequivalent cations in the MLT phase ($p = 1$ means that the TMA cation is completely ordered whereas for $p = 0$ the positions of the cations are not occupied at all). It is obvious that it is mainly only the TMA(2) cations, which in the symmetric phase are related to each other by a symmetry centre (lost at the phase transition temperature), that can contribute to the phase transition mechanism at T_C and to the spontaneous polarization. X-ray studies of both pure TMACA and TMACBA ($x = 0.42$) crystals in the MLT phase indicate some type of disorder of the TMA(2) cations. There are two possibilities: (i) the disorder is a result of the presence of a domain structure in the sample under study or (ii) the cations are not really fully ordered at room temperature and the spontaneous polarization is not saturated yet. In our opinion both explanations are possible. However, the first possibility (i) is more probable because the observed spontaneous polarization for TMACBA is nearly saturated at room temperature. In turn, the TMA(1) cations occupy the general positions in the crystal lattice and their two positions are non-equivalent. All the TMA(1) cations are dynamically disordered over the MHT phase. The process of ordering of these cations proceeds continuously with decreasing temperature over the MHT and MLT phases including the phase transition temperature. This means that the TMA(1) cations do not contribute directly to the transition mechanism at T_C because the phase transition does not influence their dynamical state. Nevertheless, it does not exclude the possibility of them making a contribution to the electric permittivity over these two phases.

The atom substitution in the anionic sublattice, i.e. either replacement of Sb atoms by Bi ones or replacement of Cl by Br, leads to a distinct decrease of the paraelectric–ferroelectric phase transition temperature. Moreover, the effect of metal substitution is stronger. The direction of change of T_C is in agreement with expectation. Both types of substitution lead to increase in the size of the $M_2X_9^{3-}$ units of the layer structure and, in consequence, to increase of the distances between the TMA(2) cations, which results in weakening of the dipole–dipole interactions. Thus, ferroelectric order appears at lower temperature in mixed crystals than in the pure analogue.

The comparison of the dynamical dielectric characteristics seems even more interesting. Generally it should be noted that all the halogenoantimonate(III) ferroelectrics with

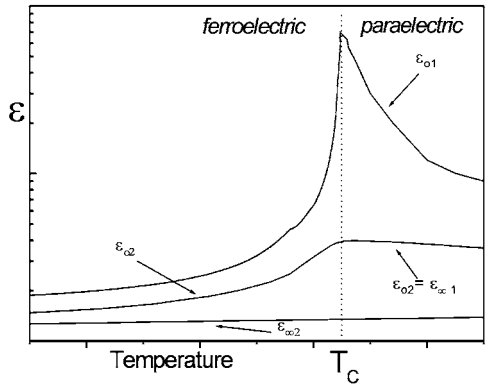

Figure 13. The contribution of the dielectric relaxators to the electric permittivity in the ferroelectric crystal TMACA.

Table 6. A schematic representation of the disorder of the trimethylammonium cations in the paraelectric (MHT) and ferroelectric (MLT) phases in TMACA and mixed ferroelectric analogues.

Monoclinic low-temperature phase (MLT) Ferroelectric Pc $(Z = 2)$	Monoclinic high-temperature phase (MHT) Paraelectric $P2_1/c$ $(Z = 2)$
(2) $p \approx 1$ 2 × TMA(2) cations (2′) $p \approx 0$	(2) $p = 0.5$ 2 × TMA(2) cations (2′) $p = 0.5$ (Cations at inversion centre)
(3) $p = 1$ 2 × TMA(3) cations (3′) $p = 0$ (1) $p = 1$ 2 × TMA(1) cations (1′) $p = 0$	 (1) $p > 0.5$ 4 × TMA(1) cations (1′) $p < 0.5$ (Cations in the general position)
All cations ordered (at RT)	All cations disordered
Six cations in the elementary cell	Six cations in the elementary cell

the anionic layer structure, $[(CH_3)_2NH_2]_3[Sb_2Cl_9]$ [33], $[(CH_3)_2NH_2]_3[Sb_2Br_9]$ [33], $[(CH_3)_3NH]_3[Sb_2Cl_9]$ [19], and their different mixed analogues, studied by the dielectric dispersion method have revealed the existence of two relaxation modes:

(i) the ferroelectric mode exhibiting strong slowing down (in the megahertz frequency region) and
(ii) the high-frequency non-ferroelectric mode active in both the paraelectric and ferroelectric phases.

The latter mode, thermally activated, is observed in a very broad frequency region (from 10^3 to 10^{10} Hz). In the case of the trimethylammonium compounds, the ferroelectric relaxation mode is assigned to the TMA(2) cations, whereas the non-ferroelectric mode should be assigned to TMA(1) or TMA(3) cations. The contribution of the dielectric relaxators to the electric permittivity is illustrated schematically in figure 13. In the case of the non-ferroelectric mixed

systems or the pure analogues TMABA or TMACB, the relaxation mode found corresponds to the non-ferroelectric mode in the ferroelectric analogues. The low dielectric strength of these relaxators ($\Delta\epsilon = 7$–15 units) suggests quite small dipole–dipole interaction in these systems. This is confirmed by the fact that the distances between interacting dipoles assigned to the TMA(2) cations in the ferroelectric systems are of the order of 6 Å, whereas in the non-ferroelectric systems the cations are separated by nearly 8.5 Å. It should emphasized that it is exclusively the dipole–dipole interactions of the cations placed inside the twelve-membered $(–Sb–Cl/Br–)_6$ rings amplified by the coupling through the anionic layer that seem to lead to the long-range order of the ferroelectric type.

Acknowledgment

This work was supported by the Polish State Committee for Scientific Research (project register 7 T09A 070 21).

References

[1] Scott J F 2000 *Ferroelectric Memories* (Berlin: Springer)
[2] Jakubas R and Sobczyk L 1990 *Phase Transit.* **20** 163
[3] Sobczyk L, Jakubas R and Zaleski J 1997 *Pol. J. Chem.* **71** 265
[4] Bator G, Baran J, Jakubas R and Sobczyk L 1998 *J. Mol. Struct.* **450** 89
[5] Varma V, Bhattacharjee R, Vasan H N and Rao C N R 1992 *Spectrochim. Acta* A **48** 1631
[6] Ishihara H, Watanabe K, Iwata A, Yamada K, Kinoshita Y, Okuda T, Krishnan V G, Dou S and Weiss A 1992 *Z. Naturf.* a **47** 65
[7] Iwata M, Eguchi M, Ishibashi Y, Sasaki S, Shimizu H, Kawai T and Shimanuki S 1993 *J. Phys. Soc. Japan* **62** 3315
[8] Ishimaru S, Suzuki K and Ikeda R 1995 *J. Phys. Soc. Japan* **64** 1754
[9] Kawai T, Ishii A, Kitamura T, Shimanuki S, Iwata M and Ishibashi Y 1996 *J. Phys. Soc. Japan* **65** 1464
[10] Gesi K, Iwata M and Ishibashi Y 1996 *J. Phys. Soc. Japan* **65** 14
[11] Kawai T, Takao E, Shimanuki S, Iwata M, Miyashita A and Ishibashi Y 1999 *J. Phys. Soc. Japan* **68** 2848
[12] Iwata M, Miyashita A, Orihara H, Ishibashi Y, Kuok M H, Rang Z L and Ng S C 1999 *Ferroelectrics* **229** 233
[13] Iwata M and Ishibashi Y 1992 *Ferroelectrics* **135** 283
[14] Iwata Y, Koyano N, Machida M, Iwata M and Ishibashi Y 2000 *Ferroelectrics* **237** 229
[15] Kuok M H, Ng S G, Tan L S, Rang Z L, Iwata M and Ishibashi Y 1998 *Solid State Commun.* **108** 159
[16] Jakubas R, Miniewicz A, Bertault M, Sworakowski J and Ecolivet C 1989 *J. Physique* **50** 1483
[17] Jakubas R, Czapla Z, Galewski Z and Sobczyk L 1986 *Ferrolectr. Lett.* **5** 143
[18] Jakubas R, Narewski E and Sobczyk L 1986 *Phys. Status Solidi* a **98** K115
[19] Bator G, Jakubas R, Zaleski J and Mróz J 2000 *J. Appl. Phys.* **88** 1015
[20] Bator G, Mróz J and Jakubas R 1997 *Physica* B **240** 362
[21] Mróz J, Pykacz H and Jakubas R 1995 *Acta Phys. Pol.* A **88** 369
[22] Mróz J and Jakubas R 1996 *Ferroelectrics* **189** 173
[23] Jakubas R, Bator G, Zaleski J, Pietraszko A and Decressain R 1996 *J. Phys.: Condens. Matter* **8** 367
[24] Sheldrick G M 1997 *SHELX-97 Program for the Solution and the Refinement of Crystal Structures* University of Gottingen, Germany
[25] Sheldrick G M 1990 *SHELXTL* (Madison, WI: Siemens Analytical X-ray Instrument Inc.)
[26] Sobiestianskas R, Czapla Z and Grigas J 1992 *Phys. Status Solidi* a **130** K69
[27] Bator G 1999 *Ferroelectrics* **223** 301
[28] Bator G, Jakubas R, Sobczyk L and Mróz J 1993 *Ferroelectrics* **141** 177
[29] Wojtaś M 2003 *Ferroelectrics* submitted
[30] Von Kruger F-J, Zettler F and Schmidt A 1979 *Z. Anorg. (Allg.) Chem.* **449** 135
[31] Adams C J and Downs A J 1972 *J. Inorg. Nucl. Chem.* **34** 1829
[32] Fomichew V V, Petrov K I, Zimina G V and Plyushchev 1973 *Russ. J. Inorg. Chem.* **18** 220
[33] Bator G and Jakubas R 1995 *Phys. Status Solidi* **147** 591